Engineering Fracture Mechanics 309 (2024) 110393

Contents lists available at ScienceDirect

Engineering Fracture Mechanics

journal homepage: www.elsevier.com/locate/engfracmech

An efficient and quantitative approach for fracture toughness measurement of Micron-Thick hard coatings based on crack spacing

Shaoyu Wu [a], Shani Yang [a], Pu Geng [b], Kewei Gao [a], Alex A. Volinsky [c], Xiaolu Pang [a,d,*]

[a] Beijing Advanced Innovation Center for Materials Genome Engineering, School of Materials Science and Engineering, University of Science and Technology Beijing, Beijing 100083, China
[b] China United Gas Turbine Technology Co., Ltd, Beijing 100015, China
[c] Department of Mechanical Engineering, University of South Florida, 4202 E. Fowler Ave. ENG030, Tampa 33620, USA
[d] Institute of Materials Intelligent Technology, Liaoning Academy of Materials, Shenyang 110010, China

ARTICLE INFO

Keywords:
Fracture toughness measurement
Hard coatings
Uniaxial tension
Multiple cracks
Residual stress

ABSTRACT

Micron-thick hard coatings find widespread applications, with fracture toughness being a crucial property that ensures their usability. However, measuring the fracture toughness of hard coatings is time-consuming and costly due to the susceptibility to cracking and small sample size. Thus, developing a simple, effective and precise measurement method is necessary. This work presents an analytical model that calculates K_C from crack spacing induced by uniaxial tension. By measuring the variation of crack spacing, this model determines the fracture toughness from the energy difference during the coating fracture, and residual stress can also be estimated. This simple method overcomes the limitations of uniaxial tension methods, does not require any in-situ observations, and offers low-cost and user-friendly testing. The K_C of TiN coatings with 2 μm thickness were tested and found to match the micro-cantilever beam test results from the literature. This model used data from other literature to calculate the toughness of diamond and a-C:H thin coatings, showing its generality. Additionally, our model's estimation of residual stress in coatings, as reported in the literature, is accurate to within 0.1 ~ 1 GPa.

1. Introduction

Hard coatings are widely used in various fields, such as cutting and molding, geology, textiles, automotive, mechanical and aerospace engineering [1–4]. Fracture toughness, a crucial service property of hard coatings, has consistently drawn extensive interest. Fracture toughness is the ability of a material to resist unstable crack propagation. In the past few decades, fracture toughness has been a key indicator to prevent catastrophic failure of structural materials [5]. Therefore, numerous studies strive to discover various ways to enhance the material's fracture toughness [6–8], which has also sparked a shared concern for the accurate evaluation of toughness. However, quantitatively measuring the fracture toughness of micron-thick hard coatings is challenging because of their thinness, brittleness and attachment to the substrate [9–12]. Therefore, despite many theoretically feasible measurement methods, it is difficult

* Corresponding author.
E-mail address: pangxl@mater.ustb.edu.cn (X. Pang).

https://doi.org/10.1016/j.engfracmech.2024.110393
Received 24 March 2024; Received in revised form 29 June 2024; Accepted 10 August 2024
Available online 13 August 2024

Nomenclature

K_C	critical stress intensity factor
G_C	critical energy release rate
U	strain energy
U_i	volumetric elastic strain energy density
U_0	strain energy of the fragment at stage-0
U_1	strain energy of the fragment at stage-1
U_2	strain energy of the fragment at stage-2
U_3	strain energy of the fragment at stage-3
U_C	theoretic fracture energy
U_f	final fracture energy
dU	Differential of crack propagation energy
dA	Differential of surface area formed by crack propagation
da	Differential of crack length formed by crack propagation
l	crack spacing
l_1	crack spacing at stage-1,
l_2	crack spacing at stage-3,
ε	strain
ε_0	Applied strain after the coating has just experienced a certain cracking
ε_f	fracture strain of coating
ε_a	applied strain
ε_{res}	residual strain of coating induced by residual stress in coating
ε_{el}	maximum elastic strain of substrate
σ	normal stress in the fragment along the x-axis
σ_1	coating stress at stage-1
σ_3	coating stress at stage-3
σ_{res}	initial residual stress in coating
σ_s	yield strength of substrate
h	coating thickness
S	substrate thickness
E_f	Young's modulus of coating
E_s	Young's modulus of substrate
$\overline{E_f}$	plane strain Young's modulus of coating
ν_f	Poisson ratio of coating
ν_s	Poisson ratio of substrate
V	the volume of the fragment
β	a dimensionless coefficient determined by the thickness of the coating and the substrate
stage-0	The stage after the coating has just experienced a certain cracking, with lower strain energy
stage-1	The stage where the coating is about to experience new cracking, with higher strain energy and unchanged crack spacing
stage-2	The stage where the coating is actively cracking, with changing strain energy and crack spacing
stage-3	The stage after the coating has completed cracking, with lower strain energy and reduced crack spacing
A	Group with large crack spacing
B	Group with medium crack spacing
C	Group with small crack spacing
D	Comprehensive group
E	Additional group
DR	residual stress derived by SDSS model
FT	fracture toughness
RS	assumed residual stress
Ave	Average fracture toughness
SD	Standard deviation of fracture toughness
SDSS	Spacing and Difference between Squares of Stresses model
HSS	High-strength steel
TiN-0.02	TiN sample with an applied strain of 2 %
TiN-0.04	TiN sample with an applied strain of 4 %
TiN-0.06	TiN sample with an applied strain of 6 %
D1	The 1st data set of Diamond coating literature's crack spacing and applied strain, details in Table 6

D2	The 2nd data set of Diamond coating literature's crack spacing and applied strain, details in Table 6
D3	The 3rd data set of Diamond coating literature's crack spacing and applied strain, details in Table 6
D4	The 4th data set of Diamond coating literature's crack spacing and applied strain, details in Table 6
D5	The 5th data set of Diamond coating literature's crack spacing and applied strain, details in Table 6
D6	The 6th data set of Diamond coating literature's crack spacing and applied strain, details in Table 6
D7	The 7th data set of Diamond coating literature's crack spacing and applied strain, details in Table 6
D8	The 8th data set of Diamond coating literature's crack spacing and applied strain, details in Table 6
a1	The 1st data set of a-C:H coating literature's crack spacing and applied strain, details in Table 6
a2	The 2nd data set of a-C:H coating literature's crack spacing and applied strain, details in Table 6
a3	The 3rd data set of a-C:H coating literature's crack spacing and applied strain, details in Table 6
a4	The 4th data set of a-C:H coating literature's crack spacing and applied strain, details in Table 6
a5	The 5th data set of a-C:H coating literature's crack spacing and applied strain, details in Table 6
a6	The 6th data set of a-C:H coating literature's crack spacing and applied strain, details in Table 6
a7	The 7th data set of a-C:H coating literature's crack spacing and applied strain, details in Table 6
a8	The 8th data set of a-C:H coating literature's crack spacing and applied strain, details in Table 6
a9	The 9th data set of a-C:H coating literature's crack spacing and applied strain, details in Table 6
a10	The 10th data set of a-C:H coating literature's crack spacing and applied strain, details in Table 6

to avoid the influence of the challenges above on sample preparation and loading, which hinders their widespread application. Micro-cantilever beam bending [13–15] and nano-indentation [16–18] are well-accepted methods in terms of evaluation mechanisms. However, micro-cantilever beam bending requires the use of FIB (Focused Ion Beam) to etch a complete micro-sized cantilever beam with a notch in the coating, followed by precise loading through in-situ nano-indentation. Therefore, the time and monetary costs of sample preparation and loading are high. Nano-indentation, to avoid the influence of the substrate, must reduce the load and thus control the indentation depth to 1/10 of the film thickness [19]. Small loads are difficult to exceed the threshold for radial crack formation in hard materials [20], and the length of radial cracks produced by indentation is a necessary parameter for calculating toughness. Therefore, the loading of nano-indentation has significant limitations. There are many similar measurement methods, but we still lack a method that is acceptable to most people in terms of sample preparation, loading, and cost, and that produces accurate results.

Reports have shown that uniaxial tension can be used as a simple and effective method to study the fracture behavior of coatings with a substrate [21–23]. Beuth et al. [24] proposed a model to determine the fracture energy release rate of coatings attached to the substrate based on uniaxial tensile loading. From this model, a simple method to measure fracture toughness without complex sample preparation and loading was derived. The buckling [25] and bending [26] methods were also based on this model. As research progressed, some studies showed that coatings develop continuous vertical cracks under large applied strain [27]. These cracks can be accurately counted and adjusted by varying the applied strain, facilitating the study of coating fracture. Researchers have linked this phenomenon with coating fracture toughness and proposed a series of models [28–32] based on the spacing between multiple cracks to improve the accuracy of the results. These models have achieved good results, and most of them have been experimentally verified. This work will utilize simple, low-cost uniaxial tension with sample preparation and loading that can be carried out with a substrate. The accuracy of the results is ensured by numerous corrections based on crack spacing. Furthermore, the method proposed in this work, based on the aforementioned models, can be applied to different strains and crack spacings within a single sample.

Although uniaxial tension is a simple method to measure coating toughness, it's easily influenced by applied strain and residual stress. Uniaxial tension mainly relies on measuring the applied strain at the time of coating fracture to evaluate toughness, according to Beuth's model [24]. Thus, an accurate fracture strain is the key. However, accurate measurement of fracture strain is challenging and requires in-situ observation, increasing testing costs. In addition, the measurement of fracture strain inevitably produces bias, and even small biases in fracture strain measurement can significantly impact the results of uniaxial tension. These studies [33–35] used in-situ observation technology to measure the fracture strain of micron-thick TiN coatings prepared by ion plating, and their bias ranged from 0.006 to 0.014. If Beuth's model is used for calculation, a strain bias of about 0.01 will cause a deviation of about 6 $MPa \cdot m^{1/2}$ in the calculated toughness, which is almost 300 % of the average toughness of TiN [13,15,36–43]. Therefore, reducing the impact of applied strain on results is a crucial challenge in improving the uniaxial tension method.

Residual stress in coatings, often comparable to or even several times the fracture stress [44,45], can significantly affect toughness measurements. Most toughness measurement methods require pre-measurement of residual stress to account for this effect and obtain intrinsic fracture toughness. Although there are many methods [44–46] to measure residual stress, the measurement undoubtedly increases the cost and reduces the efficiency of toughness measurement. Therefore, many cases [47–50] directly ignore the measurement of residual stress and determine the toughness of the coating. Ignoring residual stress can introduce bias, and a method that accurately measures toughness independent of residual stress measurement would be highly significant for thin film material research.

This work aims to develop an efficient, accurate, and low-cost measurement method based on uniaxial tension. This method will overcome the limitations of uniaxial tension being easily affected by applied strain. Additionally, this method will yield results close to intrinsic fracture toughness without considering residual stress. In this work, a model was developed to calculate K_{IC} from crack spacing induced by uniaxial tension, based on the correlation between crack spacing and fracture energy, and a test method was proposed. The results of this method are verified through comparison with experiments and literature results. The proposed method is applied to TiN coatings deposited on high-strength steel (HSS) substrates by magnetron sputtering. TiN is a commonly used hard

coating [51] that is an ideal test subject for the proposed method due to its isotropic elasticity [5], high hardness [52], brittleness [13], with a relatively stable fracture toughness range of 1.5 to 3 MPa • $m^{1/2}$ [13,15,36–43].

2. Modelling

2.1. Multiple crack formation in coatings

When uniaxial tension is applied to a ductile substrate with a brittle coating, the substrate gradually deforms, generating tensile stress. This stress is transferred to the coating through shear stress at the coating-substrate interface, resulting in the gradual accumulation of tensile stress within the coating. Eventually, the coating reaches its fracture strength, leading to coating cracking. Upon cracking, stress is released, and multiple fragments form. These fragments re-accumulate tensile stress under subsequent applied strain, leading to further cracking. This cyclic process results in multiple crack events within the original coating, with fragment sizes decreasing over time. Eventually, when the interface length between fragments and the substrate (typically comparable to the minimum crack spacing on the coating surface) becomes insufficient to transfer stress effectively, even higher applied strain won't further reduce fragment size, and coating cracking ceases. This represents the general process of multiple surface cracks in coatings. For further details, refer to the work by Bernoulli [27]. This process is characterized by identical conditions for each cracking event, except for strain, spacing, and energy differences, allowing for intrinsic fracture toughness assessment through crack spacing comparison. Consequently, our model is built on this principle, evaluating coating fracture toughness by comparing energy differences between cracked coatings based on crack spacing, rather than comparing intact coatings with cracked ones.

2.2. Determination of fracture energy and fracture toughness

To determine fracture toughness based on Griffith's criterion [53], it's necessary to obtain fracture energy. Fracture energy is the amount of energy released when a crack propagates through a coating. To obtain it, one must identify the correct component of energy during coating fracture. Assuming a coating with any length, unit width, and some thickness, ideal film-base bonding, and no crack density saturation, any additional interlayer is not considered in the modeling. Additionally, we consider that each time the applied strain reaches the fracture strain of a coating fragment, that fragment cracks and simultaneously forms multiple cracks. These cracks all develop under identical conditions, with no interaction between them. All formulas used in this work adhere to the international system of units. Fig. 1 illustrates how energy varies with crack spacing within the coating. Note that all stages depicted in Fig. 1 are during loading.

Stage 0 shows that after experiencing one or more cracking events, the coating develops cracks and releases energy in the coating. The coating is split into a fragment by cracks, which is about to be stretched further. The fragment has a crack spacing l_1 and an applied strain ε_0. Its energy is U_0, which serves as a strain energy baseline for subsequent analysis.

Next, the fragment's strain energy is raised by increasing the applied strain. At this point, the coating still retains the crack spacing resulting from the previous cracking event. Per the shear lag model for stress distribution, energy accumulates preferentially in the middle [54]. Until the applied strain reaches a certain level, there is a high strain energy in the fragment, which can meet the initiation and propagation of cracks. The fragment is about to fracture, as shown in stage 1 of Fig. 1. Applied strain for coating fracture is ε_f, and the fragment's energy is U_1.

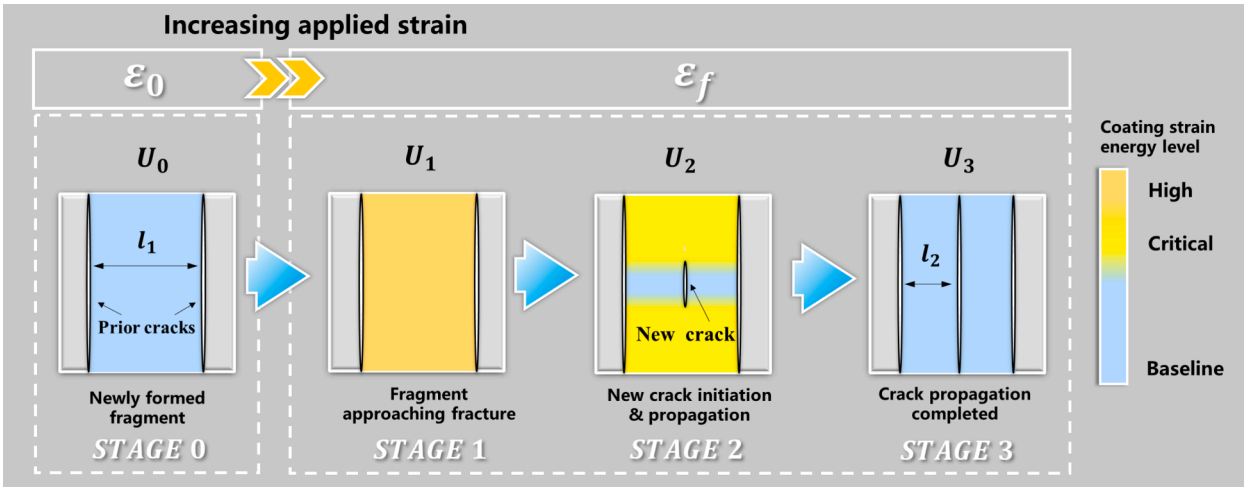

Fig. 1. A schematic diagram of the relationship between the crack spacing and the coating strain energy at each stage with increased applied strain. The theoretical fracture energy U_C is determined by the difference between the energy U_2 of the crack propagation at stage 2 and energy U_3 of the completed crack propagation at stage 3.

Under the same strain, defects in the middle of the fragment consume part of the strain energy, forming cracks, and the energy also drops in a critical level below the onset of the unstable propagation. At this time, crack tips consume strain energy and propagate, while regions where the crack passes through have energy drop to baseline level, as shown in stage 2 of Fig. 1. The applied strain remains ε_f and the fragment's energy is U_2.

When crack tips reach edge regions, the crack stops growing. A new crack splits the fragment into two new fragments with new crack spacing l_2, and strain energy drops to baseline, as shown in stage 3 of Fig. 1. Because in brittle materials, crack propagation is very fast, at this time applied strain is still ε_f, while coating has energy U_3. As a result, with increasing applied strain, coating repeats above changes, constantly producing new cracks and decreasing crack spacing. It can be found that energy consumed by crack propagation U_C should be the difference between U_2 and U_3, thus determining theoretical fracture energy $U_C = U_2 - U_3$. This energy applies to each newly formed crack.

According to Griffith's criterion and Beuth's calculation of the energy release rate for coating channel cracks [24] (i.e., the cracks in this study), the following expression defines the energy release rate of crack propagation in the coating:

$$G_C = -\frac{dU}{dA} = -\frac{dU}{h \cdot da} = \frac{U_C}{h} \tag{1}$$

Here, G_C is the critical energy release rate, dA is the new surface area formed by crack propagation, da represents the crack propagation length. In this model, da is the unit width. h is the coating thickness, and $-dU$ is replaced by U_C, where the negative sign only indicates the direction. Note that Eq.(1) theoretically applies to an individual crack. However, in this study, this equation applies to all newly formed cracks. Because we assume that all newly formed cracks follow the same conditions. Instead, K_C and G_C are related as follows:

$$K_C = \sqrt{G_C \overline{E_f}} = \sqrt{U_C \overline{E_f}/h} \tag{2}$$

K_C is the critical stress intensity factor, $\overline{E_f} = E_f/\left(1-\nu_f^2\right)$ is the plane strain Young's modulus of the coating [5,24], E_f is the Young's modulus and ν_f is the Poisson's ratio of the coating. Thus, a fracture energy-based fracture toughness formula is obtained. It should be noted that this value will be higher than the actual toughness due to the inclusion of energy of crack initiation. Despite this, it's still useful for evaluating the fracture toughness of brittle coatings. The presence of internal defects in brittle materials can reduce the energy required for crack initiation, thus minimizing this deviation.

2.3. Calculation for fracture energy

The theoretical fracture energy U_c, which determines the fracture toughness, depends on the strain energy of the fragments. Generally, U_c can be obtained by integrating the crack opening displacement function and multiplying the stress over crack propagation length [24,53,55], or integrating the critical energy release rate over propagation length [27,56]. However, these methods do not capture internal energy change due to spacing variation. Instead, the crack spacing model applies to brittle hard coatings that behave as linear elastic bodies under axial tension, producing normal stress at the cross-section of the coating. Thus, we can use the elastic strain energy equation for axial rods to calculate their strain energy. The following formula expresses the strain energy of a fragment with a given crack spacing:

$$U = U_i \cdot V = \frac{1}{2}\sigma\varepsilon \cdot V = \frac{\sigma^2 l h}{2\overline{E_f}} \tag{3}$$

Here, $U_i = \frac{1}{2}\sigma\varepsilon$ is the volumetric elastic strain energy density. V is the volume of the fragment, which has a length of l (the crack spacing), a thickness of h (the coating thickness), and a unit width. σ is the normal stress in the fragment along the x-axis. This σ is obtained by using Ahmed's model [57], which can calculate the normal stress distribution in the fragments along the uniaxial tensile direction based on the crack spacing and the applied strain. Ahmed used this model to calculate stress changes in a cracked diamond coating under uniaxial tension with a Ti substrate, which was verified experimentally. This work follows the model's assumptions: ideal bonding, no buckling or delamination, no interlayer effects, and studies a system with a brittle coating and an elastoplastic substrate. Moreover, the normal stress at the center of the fragment is chosen for calculating the strain energy in this work, because this stress is maximal according to the shear lag model [54] and Ahmed's experimental results. The stress expression is as follows [57]:

$$\sigma(l) = \left[\frac{E_f \varepsilon_{el}}{1-\nu_f^2}\left(1-\nu_f\nu_s\right)\right]\left[1-\frac{1}{\cosh\left(\frac{\beta l}{2}\right)}\right] + \left[\frac{E_f}{1-\nu_f^2}\right]\left[\varepsilon_{res}\left(1+\nu_f\right) + \left(1-\nu_f\nu_s\right)\cdot\left(\varepsilon_a - \frac{\sigma_s}{E_s}\right)\right] \tag{4}$$

Here, l is the crack spacing, E_f is Young's modulus of the coating, E_s is Young's modulus of the substrate, ε_{el} is the maximum elastic strain of the substrate, i.e. $\frac{\sigma_s}{E_s}$, ν_s is the Poisson's ratio of the substrate, β is a dimensionless coefficient determined by the thickness of the coating and the substrate, ε_{res} is the residual strain of the coating and determined by σ_{res}/E_f, σ_{res} is the initial residual stress in coating, ε_a is the applied strain, and σ_s is the flow stress of the substrate, which is substituted by the yield strength in this work. Regarding the β coefficient, the specific equation is [57]

$$\beta = \left[\frac{3}{2sh(1+\nu_s)} \left(\frac{h}{s} + \frac{\left(1-\nu_f^2\right)E_s}{(1-\nu_f\nu_s)E_f} \right) \right]^{0.5} \tag{5}$$

Here, s is the substrate thickness. For further details on establishing the stress calculation model mentioned above, interested readers are advised to refer to Ahmed's work [57]. Using Eqs. (3), (4), and (5), we can derive the strain energy expressions of the fragment at each stage, as follows:

$$U_1 = \frac{\sigma_1^2 h l_1}{2\overline{E_f}}, U_3 = \frac{2\sigma_3^2 h l_2}{2\overline{E_f}} \tag{6}$$

Here, σ_1 is the stress in the coating at stage 1, and σ_3 is the stress in the coating at stage 3. We know that l_1 represents the crack spacing at stage 1, and l_2 is the crack spacing at stage 3. Unlike l_2, which can be measured after unloading, l_1 reflects historical crack initiation and requires in-situ observation for accurate determination. Since our work does not involve in-situ observations, we assume that l_1 is twice the value of l_2, based on the shear-lag model proposed by Agrawal and Raj [54]. According to this model, stress accumulation in the coating fragments occurs primarily at the midpoint, resulting in crack initiation at that location. Consequently, the original crack spacing at stage 1 is halved due to the formation of a new crack at the midpoint. Thus, we consider l_1 to be twice the crack spacing of stage 3 ($l_1 = 2l_2$). Additionally, Ahmed's measurements of stress distribution during diamond coating tensile testing support this assumption [57]. However, it's important to note that this assumption introduces bias into our toughness calculations, as discussed in section 5.2.1. Note that the equation for U_3 has an additional factor of 2 compared to U_1, as the coating fragment is split into two parts by the new crack, which needs to be compensated for without omission in the calculated energy.

As previously stated, the theoretical fracture energy U_C requires U_2 and U_3. But U_2 is unobtainable from the above formula, as stage 2 lacks a valid crack spacing for stress calculation. Hence, an approximate treatment is to use the energy difference before and after crack propagation as a substitute [58]. In this work, the fracture energy U_C is substituted with the difference between strain energies of U_1 and U_3, denoted as the final fracture energy U_f. Since U_1 contains the energy of crack formation, U_f will be slightly larger than U_C. Therefore, the fracture energy U_f is expressed as:

$$U_f = U_1 - U_3 = \frac{\sigma_1^2 h l_1}{2\overline{E_f}} - \frac{2\sigma_3^2 h l_2}{2\overline{E_f}} = \frac{(\sigma_1^2 l_1 - 2\sigma_3^2 l_2)h}{2\overline{E_f}} \tag{7}$$

Since the previous assumption was that cracks only formed in the middle, implying l_1 always equals 2 l_2, the U_f expression simplifies to:

$$U_f = \frac{(\sigma_1^2 - \sigma_3^2)h l_2}{\overline{E_f}} \tag{8}$$

2.4. SDSS model

After obtaining the expression of fracture energy (Eq. (8)), combined with Eq. (2), the expression of coating fracture toughness based on crack spacing is obtained:

$$K_C = \sqrt{(\sigma_1^2 - \sigma_3^2) l_2} \tag{9}$$

Here, $\sigma_1 = \sigma(2l_2)$ and $\sigma_3 = \sigma(l_2)$. l_2 refers to the crack spacing after a new crack is formed, so in actual tests, it refers to the average crack spacing on the coating surface after uniaxial tension. And coating stress σ is calculated using eq. (4). It should be pointed out that the fracture strain should theoretically be based on the applied strain corresponding to the instant of new crack formation. But without in-situ observation, one cannot directly determine when the crack spacing forms. Hence, for easier calculation, the actual applied strain ε_a substitutes the fracture strain ε_f. Furthermore, it is worth noting that our model does not incorporate parameters related to initial defects or crack sizes. Unlike conventional fracture tests, which rely on measuring the propagation of individual cracks, our method determines fracture toughness by measuring the change in crack spacing. This approach emphasizes the overall fracture behavior of the coating rather than the propagation of individual cracks. Additionally, our model is based on ideal assumptions regarding coating-substrate adhesion and the brittleness of the coating. Under these assumptions, the coating naturally develops numerous cracks during uniaxial tension, without relying on pre-existing defects. Consequently, our model does not account for defect sizes.

Finally, a model that estimates $\boldsymbol{K_C}$ by considering both crack spacing and applied strain is obtained. It differs from conventional models in that it employs a form of a difference between squares of two stresses, which is represented for the strain energy difference. Hence, it is named the Spacing and Difference between Squares of Stresses (SDSS) model. The accuracy of this model will be validated by comparing it with the reference values in the literature and other characterization methods.

3. Experimental procedures

3.1. Sample preparation

Magnetron sputtering was used to deposit TiN coatings on high-strength steel. The substrates were cleaned in acetone and ethanol for 15 min each and heated to 400 °C to enhance coating crystallization. A Ti (99.995 % purity) target was used with DC reactive magnetron sputtering at 150 W power to deposit TiN coating on a high-strength steel substrate. The substrate was etched for 10 min at −900 V bias voltage under 1.5 Pa Ar gas, then a Ti transition layer was deposited under 0.6 Pa Ar gas, followed by a TiN layer under 0.6 Pa N_2/Ar gas mixture (6 sccm/20 sccm) at 400 °C for 3 h. A −50 V bias voltage was applied during deposition to obtain dense coatings. The substrate material is high-strength steel (HSS) with the 815 MPa yield strength, 206 GPa Young's modulus, and 0.3 Poisson's ratio, which was cut into dog-bone tensile samples with 0.8 mm thickness, 40 mm length, 10 mm gauge and 4 mm width (see Fig. 5(a)), where the coating was deposited at the gauge length with both ends masked. The coating is also deposited on Si wafers, primarily for obtaining scanning electron microscopy (SEM) images to determine coating thickness and morphology. The coating process is similar to that used for the HSS substrate.

3.2. Characterization methods

The hardness and Young's modulus of coatings were measured using a TI-900 in-situ nanomechanical testing system from Hysitron, USA, loaded with a Berkovich indenter tip with a maximum load of 10 mN and a maximum indentation depth of about 120 nm. These measurements were performed on coatings attached to HSS substrates. The surface and cross-sectional morphology of the coatings were characterized by a Zeiss EVO-18 field emission scanning electron microscopy. The cross-sectional samples were obtained by manually fracturing the coating adhered to silicon wafers, followed by SEM observation. The elemental composition of TiN was determined using energy-dispersive X-ray spectroscopy (EDS) equipped on the scanning electron microscope.

Crack spacing in the coating was measured by counting cracks on the unloaded surface using a Leica DM2500 M materials analysis microscope. Notably, we did not consider any changes in crack spacing after unloading. In this work, crack spacing statistics were conducted as follows: the average crack spacing for each sample is calculated by taking 3 photos of different surface locations and counting the average crack spacing at 3 different horizontal lines in each photo. The highest and lowest values among the 9 crack spacings are discarded and the remaining values are averaged to obtain the final average crack spacing. Fig. 2 is an example of a statistical image for average crack spacing. The a, b, and c represent the lines selected for crack spacing measurement, with more lines being used in actual statistics. The selection of these lines should cover the entire field of view, and both the start and end of each line must be in contact with a crack. Subsequently, count the number of cracks that cross the line (excluding the last crack contacted by the horizontal line), and calculate the crack spacing by dividing the length of the line by the number of cracks. In Fig. 2, the crack spacings for lines a, b, and c are 35.7 μm, 36.4 μm and 37.3 μm, respectively. Thus, the image yields three measurements of crack spacing. Then, move horizontally left or right to capture at least 2 additional images from different positions. The positions should be as close as possible to the center of the coating, with the densest distribution of cracks. There are no additional requirements for magnification, but at least 5 cracks must be visible in the field of view. Follow the same procedure for the other 2 images to obtain 3 additional measurements of crack spacing each, resulting in a total of nine measurements. Exclude the highest and lowest values from the 9

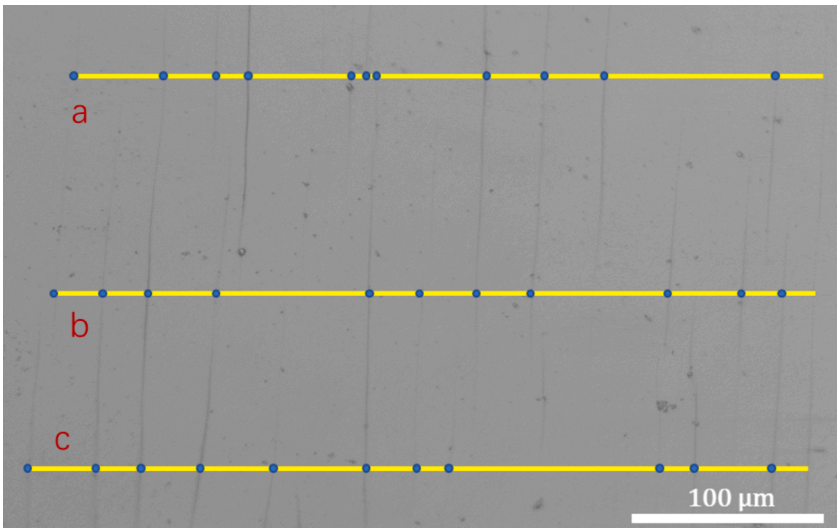

Fig. 2. Example of crack spacing measurement. The depicted crack spacing is not associated with the data of this study, and blue dots represent the cracks intersected by the dashed lines. (For interpretation of the references to colour in this figure legend, the reader is referred to the web version of this article.)

measurements, and calculate the average of the remaining values to determine the final average crack spacing.

3.3. Tensile test

The uniaxial tension test was carried out using the CMT2303 Electromechanical Test Systems from MTS SYSTEMS Co., Ltd. The applied strain was controlled by the original extensometer from this manufacturer (with a maximum range of 20 mm). In this work, tests with different applied strains were conducted, which resulted in different average crack spacings, to check the consistency of the results obtained by this method. The choice of applied strain should balance the need for sufficient crack spacing in the TiN coating and the risk of saturation that leads to coating delamination and spalling, which would compromise the study of coating fracture. Based on previous research [33], the applied strain values were set at 2 %, 4 %, and 6 %. The tensile rate was 0.1 mm/min, and the samples are shown in Table 1.

4. Results

4.1. The coating morphology, thickness and mechanical property

The cross-sectional morphology of the TiN coatings, as well as their dense columnar crystal structure without apparent defects, are displayed in Fig. 3(a). A Ti transition layer with a thickness close to 100 nm and a TiN coating with a thickness close to $2\mu m$ are marked in Fig. 3(a). The surface morphology is shown in Fig. 3(b). Fig. 3 illustrates the typical morphology of TiN coatings prepared via magnetron sputtering. Furthermore, the elemental composition of the coating is shown in Table 2, confirming that the prepared TiN is stoichiometric.

The load-depth curves, shown in Fig. 4, were used to calculate the average hardness and Young's modulus of the TiN coatings using Oliver and Pharr's method [59]. Three indentations were performed at different locations for each sample, with a maximum load of 10 mN, 10 s loading time, and 2 s peak load holding time. The maximum indentation depth for all indents was controlled to be 1/10 of the coating thickness to avoid the influence of the substrate. The Young's modulus of TiN was found to be $320.3 \pm 4.1 GPa$, while the hardness was 26.4 ± 1.1 GPa.

4.2. Applied strain and crack spacing

Fig. 5 presents the stress–strain data for coated specimens with a thickness of 0.8 mm. For the uncoated substrate, a yield stress of 750–830 MPa is observed, typical for this type of steel. The extensometer functioned properly, with all samples showing a maximum strain value differing by less than 1 % from the target value, indicating that the applied strain met the intended design target. In this study, to ensure effective strain transfer from the substrate to the coating, a 100 nm thick Ti interlayer was deposited to enhance the adhesion between the film and the substrate, thus fulfilling the hypothesis of ideal stress transfer. Poor adhesion can impede stress transfer within the coating, inhibiting the formation of crack spacing and potentially leading to premature delamination rather than cracking. Consequently, the interlayer is regarded as an ideal bonding interface in this work, with our model not accounting for the specific role of the interlayer. For more detailed insights into the role of the interlayer in stress transfer, please refer to the following studies [57,60]. Additionally, for readers interested in the mechanism by which substrate strain affects coating strain, it is recommended to consult the following studies [27,54]. In essence, substrate deformation transfers stress to the coating through shear stress at the interface, with a stress transfer length that limits the stress transfer in the coating and thereby controls the variation in crack spacing. This section will not elaborate further.

The distribution and statistics of crack spacing on the surface of each coating are shown in Fig. 6. A local view of the TiN-coated surface is displayed in Fig. 6(a). No peeling or crumbling of the coating was observed after loading, indicating good adhesion properties. The cracks on the coating surface were vertical and perpendicular, suggesting the brittleness and uniformity of the coating. The average crack spacing results for the TiN-coated samples were given in Fig. 6(b), and a gradual decrease in crack spacing was observed with increasing strain, which followed the general trend [32,33,61]. It should be noted that we believe residual stresses do not affect the size and variation of these crack spacings. Ahmed's in-situ tensile tests [57] have confirmed that the residual stresses in the coating are significantly relieved by the plastic deformation of the substrate. They measured the internal stress of diamond coatings after 1 % applied strain (at which the coating first cracked) using Raman spectroscopy. The results showed that the internal stress after unloading was only −1 GPa, much lower than the initial residual stress of −5.4 GPa when the coating was not loaded. For specific details, one can refer to their work [57]. Since the residual stress in the coating is relieved by the plastic deformation of the substrate, the cracking of the coating occurs without residual stress, thus the size and variation of the crack spacing are not influenced by residual

Table 1
Material systems and maximum applied tensile strain for each sample.

Sample number	Coating material	Substrate material	Maximum tensile strain
TiN-0.06	TiN	HSS	6 %
TiN-0.04	TiN	HSS	4 %
TiN-0.02	TiN	HSS	2 %

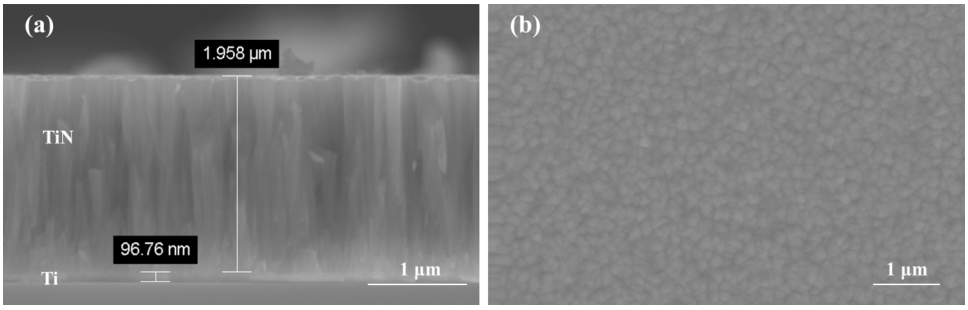

Fig. 3. Surface and cross-sectional morphology of TiN coating with annotated thickness of coating and transition layer. (a) cross-sectional view, (b) surface view.

Table 2
Elemental composition of the investigated coating obtained by EDS.

Element	At%
N	45.47
Ti	42.99
O	9.56
Si	1.41
Al	0.43
Ni	0.1
Ar	0.04

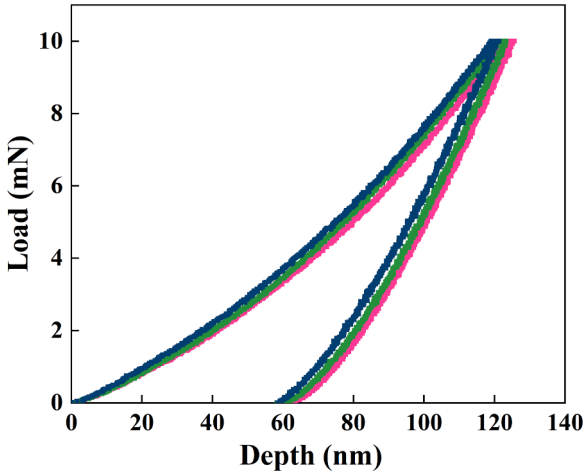

Fig. 4. TiN coating nanoindentation load–displacement curves.

stress. Additionally, the research by Rehman et al. [60] also indicates that coatings under uniaxial tension need to release residual stress before cracking or delamination occurs. Therefore, although this study did not measure the residual stress, the results of these crack spacings are credible.

4.3. K_C results

Since the samples in this work were prepared under the same process and batch, they share the same toughness and residual stress. Thus, we could propose a strategy that not only provides the toughness of the samples without knowing residual stress but also estimates their residual stress. We initially assign the same residual stress value to TiN-0.02, TiN-0.04, and TiN-0.06, calculate their toughness using the SSDS model (Eq.(9)), and then calculate the standard deviation of these toughness values. Subsequently, we replace the residual stress with other values and recalculate the toughness and standard deviation. This process is repeated until the smallest standard deviation is obtained. The toughness corresponding to this standard deviation is the final result. Table 3 presents the data used in our calculation of TiN toughness, and the Poisson's ratio of the TiN is 0.21[5].

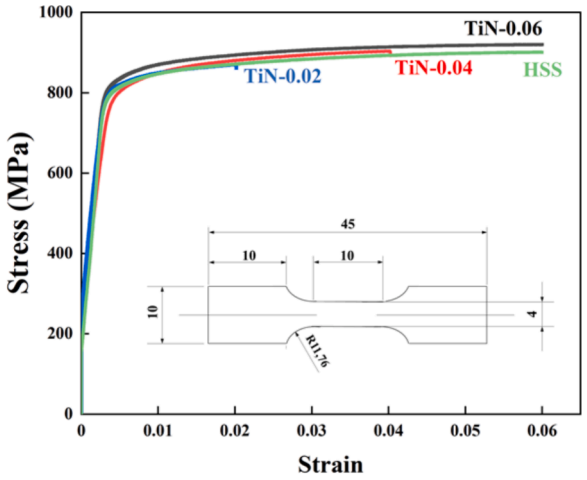

Fig. 5. Stress–strain curves for all coated samples and the substrate, as well as parameters for dog-bone tensile specimens.

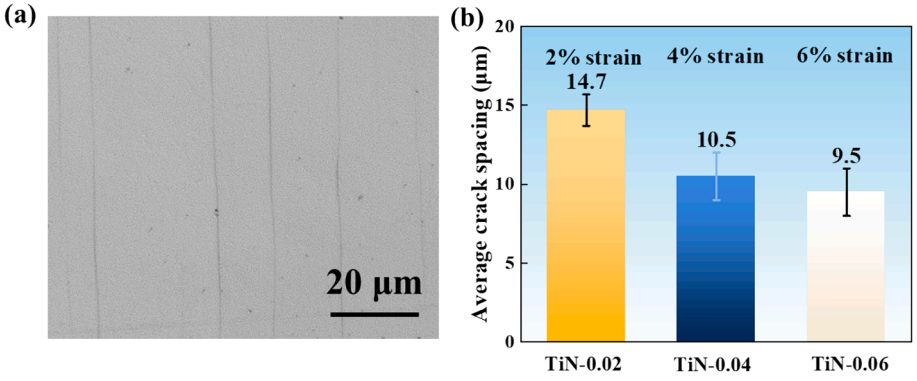

Fig. 6. Optical image and statistics of average crack spacing of the coatings: (a) TiN surface cracks morphology with $\varepsilon_a = 2\%$. (b) crack spacing of TiN coating with different strains on HSS substrates.

Table 3
Parameters for calculating the Toughness of TiN Samples, and the Poisson's ratio of the coating is 0.21 [5].

No.	Substrate	h, Î¼m	s, Î¼m	ν_f	ν_s	E_f, GPa	E_s, GPa	σ_s, MPa	ε_a	l_2, Î¼m
TiN-0.02	HSS	2	1000	0.21	0.3	320	206	815	0.02	14.7
TiN-0.04									0.04	10.4
TiN-0.06									0.06	9.4

Table 4
The results of toughness and standard deviation of TiN samples under residual stress from −3.5 to + 1 GPa. Except for the SD column, the other results retain only one decimal place. The subsequent tables from Tables. 5, 7 and 8 also adopt these descriptions and treatments.

RS	TiN-0.02	TiN-0.04	TiN-0.06	ave	SD
+1	2.9	2.5	2.6	2.7	0.22
+0.5	2.8	2.4	2.6	2.6	0.18
0	2.6	2.3	2.5	2.5	0.13
−0.5	**2.4**	**2.3**	**2.5**	**2.4**	**0.10**
−1	2.3	2.2	2.4	2.3	0.11
−1.5	2.1	2.1	2.4	2.2	0.17
−2	1.8	2.1	2.3	2.1	0.24
−2.5	1.6	2.0	2.3	2.0	0.34
−3	1.3	1.9	2.2	1.8	0.47
−3.5	0.9	1.8	2.2	1.6	0.65

We initially selected a range of residual stress from −3.5 to 1 GPa with an increment of 0.5 GPa. The reason for not choosing a larger compressive stress is that the toughness results would become imaginary, rendering them invalid. The results are presented in Table 4, where the "-" symbol denotes compressive stress and the "+" symbol denotes tensile stress. It was found that the toughness with a standard deviation minimum occurred at a residual stress of −0.5 GPa. We then refined the range of residual stress with an increment of 0.1 GPa and further calculated the standard deviation of toughness, as shown in Table 5. Ultimately, we determined the average fracture toughness at a residual stress of −0.6 GPa, 2.4 $MPa \cdot m^{1/2}$, as the final fracture toughness. This result is very close to the reference value of $2.3 \pm 0.3\ MPa \cdot m^{1/2}$ [13,15,36–43], which was obtained by the micro-cantilever method, and the samples were magnetron-sputtered coatings with film thicknesses ranging from 1 to 4 μm, ensuring comparability. For the TiN-coated samples with different applied strains and crack spacings, their results also showed high consistency, with less than a 5 % difference between the three samples. Therefore, this result demonstrated the feasibility of this method for the quantitative evaluation of fracture toughness.

However, this study did not measure the residual stress of the coating, and thus cannot solely validate the current results now. Therefore, we will employ the SSDS model and this strategy, utilizing data from other literature that has measured residual stress, to calculate their toughness and verify the accuracy of the assumed residual stress and toughness. The data is acquired from literature involving multiple cracking research or fragment analysis in a hard coating. These researches focused on the fracture behavior within a specific material system without additional improvements to the prepared coatings. We believe that the properties of these coatings should fall within a general range and can serve as validation subjects for this model. Due to the scarcity of relevant literature or available data, only the results for diamond [60] and a-C:H [62] coatings were obtained. Their data come from in-situ tensile tests on individual samples, so the residual stress effects and toughness at different strains should also be consistent (the influence of residual stress on strain will be discussed later). In the literature, all data except for the crack spacing and the applied strain at the first cracking were used, without any manual selection. The data for the first cracking can only be used to compare the energy between intact and cracked coatings, which does not align with the concept of this model, which is to compare the energy between cracked coatings. The relevant literature data used for calculations have been presented in Table 6. The results of this strategy's calculations are shown in Tables 7 and 8, where the assumed residual stress is denoted by RS, ave represents the average toughness, and SD represents the standard deviation of toughness. These notations will also be used for expressions appearing later in this paper.

To simplify the content, only the results with a search step of 0.1 GPa are shown, and all results have been searched over the range of −10 to 2 GPa. The results for diamond are shown in Table 7. When the residual stress is −5.5 GPa, the standard deviation of the diamond coating's toughness is the smallest, with an average fracture toughness of 7.6 $MPa \cdot m^{1/2}$, close to the reported toughness of diamond: 8.4 $MPa \cdot m^{1/2}$ [63,64], which was obtained through three-point and four-point bending. Moreover, the actual residual stress of this diamond coating is −5.4 GPa, very close to the −5.5 GPa derived by this model. The results for the a-C:H coating are shown in Table 8. When the residual stress is −1.8 GPa, the standard deviation of the a-C:H is the smallest, with an average fracture toughness of 1.8 $MPa \cdot m^{1/2}$. It is close to the fracture toughness of 1.8 MPa • $m^{1/2}$ for a-C:H thin film obtained by Schaufler et al. [65] using micro-cantilever bending. The residual stress of this a-C:H coating is −1 GPa, also very close to the −1.8 GPa derived by this model. Through the aforementioned results, we can observe that the assumed residual stress deviates from the actual residual stress by a minimum of 0.1 GPa and a maximum of 0.8 GPa. The calculated toughness shows a maximum deviation from the reference value of 0.6 MPa • $m^{1/2}$, with the minimum deviation being close to 0. In summary, the SDSS model, combined with this strategy, has demonstrated surprising accuracy. Therefore, we believe that the fracture toughness and residual stress obtained through this strategy are valid.

5. Discussion

5.1. The impact of sample data selection on results

In Section 4.3, we demonstrate the accuracy and consistency achieved in calculating the toughness and residual stress of multiple samples using the SDSS model under conditions of unknown residual stress. However, the results obtained from literature data are supported by at least 8 different data samples with varying strain and crack spacing, whereas the TiN samples only have 3 different strains and crack spacings. Therefore, we will continue to discuss the impact of using only 3 different data samples on the results, based on data from diamond coating and a-C:H coating.

Table 5
The results of toughness and standard deviation of TiN samples under residual stress from −1 to 0 GPa.

RS	TiN-0.02	TiN-0.04	TiN-0.06	ave	SD
0	2.6	2.3	2.5	2.5	0.1312
−0.1	2.6	2.3	2.5	2.5	0.1235
−0.2	2.5	2.3	2.5	2.4	0.1166
−0.3	2.5	2.3	2.5	2.4	0.1107
−0.4	2.5	2.3	2.5	2.4	0.1059
−0.5	2.4	2.3	2.5	2.4	0.1026
−0.6	**2.4**	**2.3**	**2.5**	**2.4**	**0.1010**
−0.7	2.4	2.2	2.5	2.4	0.1012
−0.8	2.3	2.2	2.4	2.3	0.1034
−0.9	2.3	2.2	2.4	2.3	0.1076
−1	2.3	2.2	2.4	2.3	0.1136

Table 6
The parameters obtained from the literature[60,62].

No.	Coating	Substrate	h, Î¼m	s, Î¼m	ν_f	ν_s	E_f, GPa	E_s, GPa	σ_s, MPa	σ_{res}, GPa	ε_a	l_2,Î¼m	Reference
D1	diamond	Ti	1.5	100	0.07	0.34	1200	104	340	−5.4	0.0055	309.2	[60]
D2											0.0059	188	
D3											0.0065	85.1	
D4											0.0072	54.4	
D5											0.008	35.2	
D6											0.0085	30.7	
D7											0.0095	25.4	
D8											0.012	20.3	
a1	a-C:H	steel	1.9	100	0.2	0.3	150	210	240	−1	0.021	24.2	[62]
a2											0.028	15.4	
a3											0.035	13.3	
a4											0.042	12.8	
a5											0.05	10.5	
a6											0.055	9.7	
a7											0.063	8.5	
a8											0.07	7.7	
a9											0.077	6.3	
a10											0.084	5.5	

Table 7
The results of diamond coating under residual stress from −5.7 to −5 GPa. The data used are from the literature[60], and the actual residual stress is −5.4 GPa. D1 to D8 correspond to the same numbers in Table 6.

RS	D1	D2	D3	D4	D5	D6	D7	D8	ave	SD
−5	8.2	15.8	14.3	10.9	8.2	8.2	8.4	9.1	10.4	3.03
−5.1	7.8	15.1	13.4	10.1	7.7	7.9	8.2	9.0	9.9	2.82
−5.2	7.3	14.4	12.4	9.3	7.3	7.6	8.0	8.9	9.4	2.60
−5.3	6.8	13.6	11.2	8.4	6.8	7.3	7.8	8.8	8.9	2.40
−5.4	6.3	12.8	10.0	7.4	6.3	6.9	7.6	8.8	8.3	2.22
−5.5	**5.7**	**12.0**	**8.6**	**6.3**	**5.7**	**6.6**	**7.4**	**8.7**	**7.6**	**2.10**
−5.6	5.1	11.0	6.9	4.9	5.1	6.2	7.2	8.6	6.9	2.11
−5.7	4.3	10.0	4.6	2.8	4.4	5.8	7.0	8.5	5.9	2.41

Table 8
The results of a-C:H coating under residual stress from −2 to −1 GPa. The data used are from the literature[62], and the actual residual stress is −1 GPa. a1 to a10 correspond to the same numbers in Table 6.

RS	a1	a2	a3	a4	a5	a6	a7	a8	a9	a10	ave	SD
−1	2.3	2.2	2.3	2.5	2.2	2.1	2.0	1.9	1.5	1.3	2.0	0.362
−1.1	2.2	2.1	2.2	2.4	2.2	2.1	2.0	1.9	1.5	1.3	2.0	0.347
−1.2	2.2	2.1	2.2	2.4	2.2	2.1	2.0	1.8	1.5	1.3	2.0	0.333
−1.3	2.1	2.0	2.1	2.4	2.1	2.1	1.9	1.8	1.5	1.3	1.9	0.320
−1.4	2.0	2.0	2.1	2.3	2.1	2.1	1.9	1.8	1.5	1.3	1.9	0.308
−1.5	1.9	1.9	2.1	2.3	2.1	2.0	1.9	1.8	1.5	1.3	1.9	0.298
−1.6	1.8	1.9	2.0	2.3	2.1	2.0	1.9	1.8	1.5	1.3	1.8	0.290
−1.7	1.7	1.8	2.0	2.2	2.1	2.0	1.9	1.8	1.5	1.3	1.8	0.286
−1.8	**1.5**	**1.8**	**1.9**	**2.2**	**2.0**	**2.0**	**1.9**	**1.8**	**1.4**	**1.3**	**1.8**	**0.285**
−1.9	1.4	1.7	1.9	2.1	2.0	2.0	1.8	1.7	1.4	1.3	1.7	0.290
−2	1.3	1.6	1.8	2.1	2.0	1.9	1.8	1.7	1.4	1.2	1.7	0.301

Table 9
The specific compositions of Groups A, B, C, D, and E. The serial numbers in this table correspond to those in Table 6.

Groups	Diamond	a-C:H
A	D1, D2, D3	a1, a2, a3
B	D3, D4, D5	a4, a5, a6
C	D6, D7, D8	a8, a9, a10
D	D2, D4, D7	a2, a5, a9
E	D5, D7, D8	a2, a5, a6

We selected five sets of sample data, designated as the Large Crack Spacing Group (Group A), Medium Crack Spacing Group (Group B), Small Crack Spacing Group (Group C), Comprehensive Group (Group D), and Additional Group (Group E). The primary distinction among them lies in the variation of crack spacing. Group A consists of the top 3 samples with the largest crack spacings, Group C of the top 3 with the smallest, and Group B includes 3 samples with spacings intermediate between those of Groups A and C. The Comprehensive Group is composed of one intermediate sample from each of the A, B and C groups. The Additional Group is formed by selecting samples from the literature data that closely resemble the crack spacing ratios (14.7:10.4:9.4) observed in the TiN samples, primarily to verify whether the results of TiN exhibit significant deviations. Each group contains 3 samples, with specific details available in Table 9. After the selection of the sample data, we calculated the corresponding residual stress, average fracture toughness, and standard deviation according to the strategy proposed in Section 4.3, and observed the discrepancies between these values and the actual reference values for residual stress and fracture toughness. The results are depicted in Fig. 7(a) and (b), where FT stands for fracture toughness.

Fig. 7(a) and (b) allow us to draw three conclusions. First, without knowledge of the residual stress, Groups A, B, and C are not suitable for selecting sample data in actual testing. Second, with unknown residual stress, Group D is recommended for data selection in actual testing. Third, the likelihood of significant deviation in the TiN results obtained in this study is low. Explanations will now follow.

Among the two coatings, the approximate residual stress and fracture toughness derived from Group A is close to the target values. However, large crack spacing implies that testers must ensure the applied load is near the point of initial fracture of the coating. This requires sufficient experience from the testers, as the initial fracture is highly influenced by the coating's initial state (initial residual stress, initial defects, etc.). If we lack experience or wish to test new materials, in-situ observation methods are essential. In either case, the cost of testing is significantly increased, thus making the selection method of Group A not recommended.

Groups B and C show significant deviations in estimating fracture toughness and residual stress. Group B exhibits a notable deviation in the toughness estimation of diamond, approximately 4.5 MPa • $m^{1/2}$, with a deviation percentage of about 54 %. Group C's estimation of residual stress and toughness for a-C:H reaches deviations of around 6 GPa and 1 MPa • $m^{1/2}$, respectively, with deviation percentages of approximately 600 % and 56 %. Therefore, the selection methods of Groups B and C are also inadvisable.

Group D performs better, with estimates of residual stress and toughness being close to the target values. Although Group D shows a 1 GPa deviation in the estimation of residual stress for the a-C:H coating, it does not cause a significant deviation in toughness. Moreover, the data obtained in Group D are more in line with actual testing conditions, i.e., a wide range of applied strains, whereas Groups A, B, and C have a very narrow range of applied strains.

Finally, Group E shows results very close to the target values. Therefore, from the perspective of crack spacing variation, it indicates

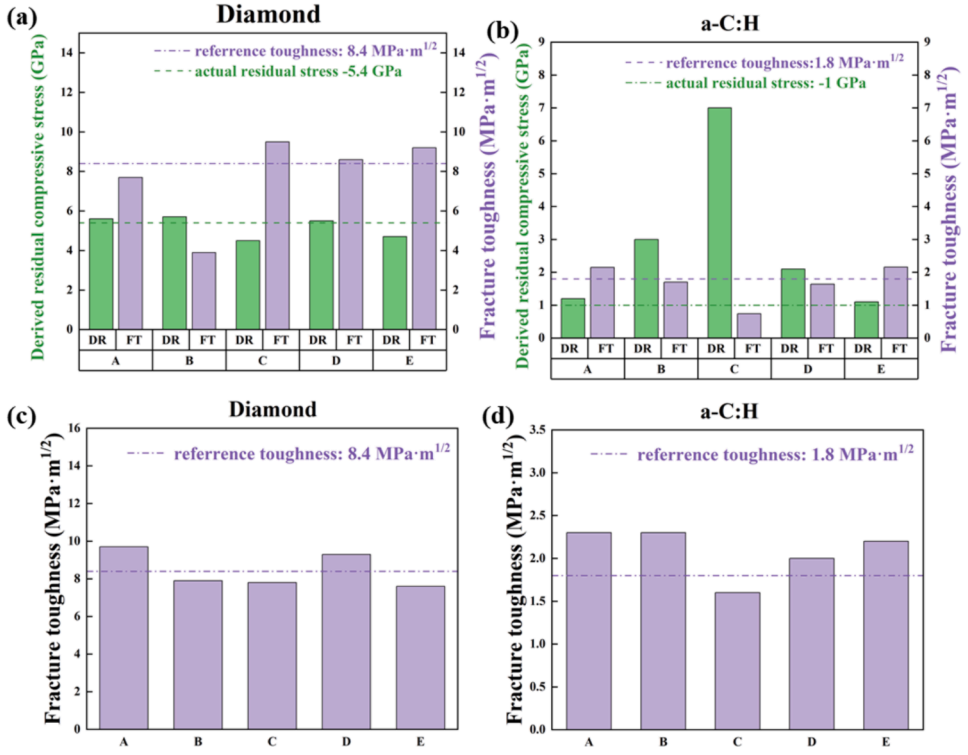

Fig. 7. Calculated residual stress and toughness from sample data with varying crack spacing. DR indicates derived residual stress (all compressive, hence no "-" sign on the y-axis), and FT denotes calculated fracture toughness. (a) and (b) are without known residual stress; (c) and (d) with known actual residual stress.

that the likelihood of significant deviation in the TiN results obtained in this study is low.

Although we have discussed the optimal crack spacing for obtaining accurate results, we found significant deviations in Groups B and C. Therefore, we will discuss the possible causes of these deviations. The main deviation in Group C stems from the estimation of residual stress, which in turn leads to an incorrect estimation of toughness. Hence, it is necessary to discuss the impact of residual stress on the SDSS model. The influence of residual stress on the SDSS model is primarily through the applied strain. Generally, tensile residual stress promotes the strain at which the coating fractures, while compressive residual stress inhibits it. The inhibition manifests as a higher absolute applied strain required for all cracking, leading to an overestimation of toughness calculated by the SDSS model. This deviation in applied strain caused by residual stress is denoted as ε_{res}, or residual strain in Eq. (4). To express the applied strain free from the influence of residual strain, it can be represented as $(\varepsilon_a - \varepsilon_{res})$. However, this deviation is limited because the residual stress will permanently decrease with the increase of substrate plastic deformation. Ahmed's in-situ tensile tests [57] have confirmed that the residual stress in the coating is significantly released by substrate plastic deformation. Therefore, as long as the applied strain is large enough, the applied strain unaffected by residual stress $(\varepsilon_a - \varepsilon_{res})$ can equal the strain affected by residual stress ε_a, significantly reducing this deviation. This can be confirmed by comparing the toughness variations in the small applied strain column (TiN-0.02) and the large applied strain column (TiN-0.06) in Table 4. The variation range of toughness corresponding to large applied strains under different residual stress conditions (2.2 to 2.6 MPa $\bullet$ $m^{1/2}$) is significantly smaller than that of small strains (0.9 to 2.9 MPa $\bullet$ $m^{1/2}$), and other tables show the same trend.

What is the relationship between this effect and the residual stress deviation caused by Group C? Since Group C has a larger applied strain, the impact of residual stress is smaller, which is not conducive to the SDSS model sensing the influence of residual stress, making it difficult to deduce the actual residual stress. In contrast, Groups A, D, and E have data with smaller applied strains. These data are more significantly affected by residual stress, which can help the SDSS model sense the effect of residual stress, thereby deducing results closer to the actual residual stress. Therefore, to assess residual stress using the strategy proposed in Section 4.3, one should avoid the sampling method of Group C and include sample data with small applied strains as much as possible. The cause of the error in Group B is not yet clear to us, and further in-depth research is needed to reveal it. However, we can avoid the sampling method of Group B and, in addition to following the method of Group D, we can also increase the number of samples, i.e., increase the sample data to reduce the impact of Group B, similar to Tables 7 and 8, where results obtained from more than 8 samples are also ideal.

Additionally, the aforementioned results are based on the premise of unknown residual stress. The toughness obtained under the condition of known residual stress is plotted in Fig. 7(c) and (d). It can be observed that for both diamond coating and a-C:H coating, Groups A, B, C, D, and E all exhibit relatively consistent results, which are also close to the reference toughness values. Therefore, although it is possible to proceed without measuring the residual stress, more robust results can be obtained when the residual stress is accounted for.

5.2. Limitations of this method

5.2.1. Estimation of crack spacing

When considering the change in crack spacing due to coating cracking under the same strain, we proposed, based on the shear lag model [54] and experimental results from Ahmed [57], that the old crack spacing is twice the new one, denoted as $(l_1 = 2l_2)$. However, this relationship is only applicable when the applied strain is relatively small. As the applied strain increases and the crack density approaches saturation, the change in crack spacing will diminish, making it difficult to maintain the 2x relationship. Additionally, due to the non-uniform in coating properties, loading, and deformation, some parts of the coating do not produce new cracks. These areas may require more applied strain to crack, delaying the reduction in crack spacing. If these spacings are included in the statistics, it will lead to an overestimation of the measurements. Consequently, under larger strains, both l_1 and l_2 are biased high, which in turn leads to overestimated results. However, this effect is limited. The smaller the measured crack spacing (i.e.,l_2), the smaller l_1 will be, reducing the deviation. Therefore, in this study, the results obtained with larger applied strains did not show a deviation larger than the reference values.

To mitigate this effect, a feasible approach is to identify the area with the densest crack distribution when measuring crack spacing, which is typically located at the center of the coating. However, this location can also vary due to the actual uneven performance of the brittle coating or asymmetric sample clamping. Therefore, we need to search for areas with dense crack distribution in and around the center. In this study, although the crack spacing measured came from dense areas, the deviation still exists and requires further research to address the issue. Moreover, we cannot easily change the 2x relationship, as it simplifies the determination of the coating energy. Changing it to another relationship would make the variation in coating energy difficult to ascertain, complicating the modelling.

5.2.2. Estimation of fracture strain

In this method, the strain used in calculating the toughness of TiN samples is the overall strain. In reality, the fracture strain should be used, which corresponds to the applied strain at the time of crack spacing generation. The reason for this discrepancy is the absence of in-situ observation capabilities. This results in an overestimation of the fracture strain and, consequently, an overestimation of toughness. To account for this effect, we plotted a heatmap of the toughness variation calculated by the SDSS model within a certain range of applied strain and crack spacing, with the residual stress set at −0.6 GPa and other necessary parameters for the calculation derived from the TiN samples, which are the parts in Table 3 excluding crack spacing and applied strain. The range of crack spacing is set from 4 to 20 μm, and the range of applied strain is set between 0.01 and 0.1. In Fig. 8, brightness represents toughness; significant

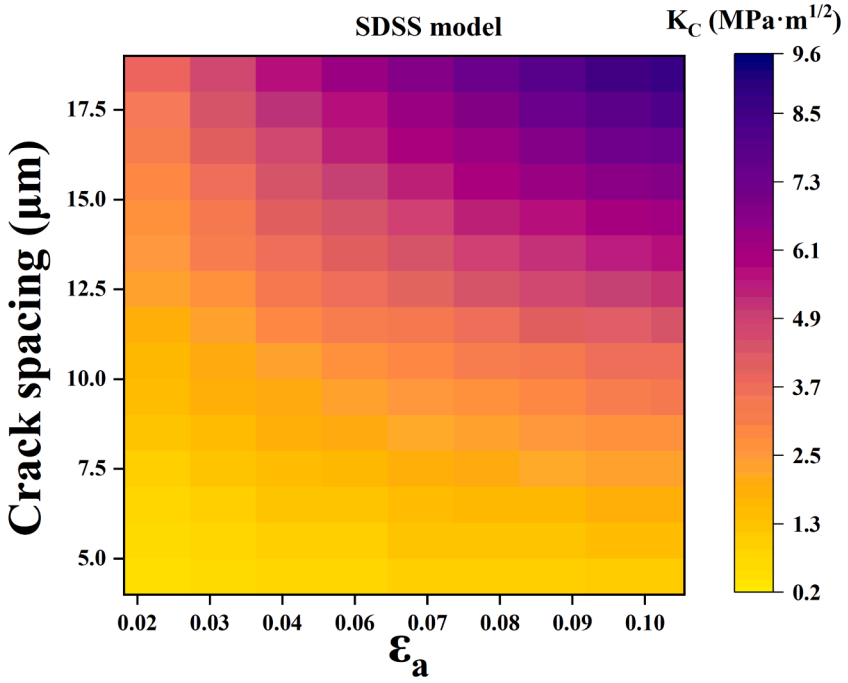

Fig. 8. The effect of applied strain on the results of the SDSS model. The variation in brightness within the figure signifies the change in fracture toughness as determined by the SDSS model.

changes in brightness indicate large variations in toughness, while similar brightness suggests minimal variation. From Fig. 8, we can observe that as the crack spacing decreases, the impact of applied strain on the results diminishes, as indicated by the diminishing changes in brightness, suggesting that the variation in toughness also becomes smaller. Therefore, we believe that this effect is not particularly significant, at least for the crack spacing in the TiN samples in this study.

5.3. Restrictions

The applied strain needs to be restricted. First, as applied strain increases, the crack spacing of the coating decreases until it saturates [66]. Then, the further strain does not affect crack spacing but causes coating peeling and detachment. Hence, excessive strain loses its correlation with crack spacing and fails to show the fracture ability of the coating.

A strong adhesion is necessary. To ensure accurate stress calculation, it's crucial to prepare a coating with strong adhesion. The interface adhesion transfers substrate deformation to coating, but the lower adhesion property worsens the transfer effect and increases coating crack spacing, thus affecting the results. Therefore, the interface adhesion should remain strong throughout the test, and secondary cracking and buckling-induced delamination are not permissible. In this work, magnetron sputtering was used to prepare the coating due to its excellent adhesion performance. Thus, although adhesion is important, this model lacks consideration of the specific role of the transition layer, which should become an important issue in future research.

The thickness of the coating needs to be restricted. Coating thickness also influences this model significantly, as it affects crack spacing. The shear-lag model theory suggests a proportional relationship between coating thickness and crack spacing due to stress transfer length [67,68], and coating thickness also determines when saturated crack spacing appears under large strain [27]. Most studies on coating fracture through crack spacing have limited the coating thickness to within 5 μm. Therefore, to ensure the effectiveness of this method, it can only be applied to coatings with a thickness of less than 5 μm.

The substrate material must possess adequate strength and good toughness. A substrate with a higher yield strength can ensure that the coating cracks promptly, with this strength being at least comparable to that of stainless steel. According to Rehman's work [60], the higher the yield strength of the substrate, the greater its capacity to transfer stress to the coating, allowing the coating to crack at an earlier strain. Conversely, a softer substrate will delay the transfer of stress to the coating, inhibiting the cracking and variation in crack spacing of the coating. Moreover, the primary part of the model used to calculate the coating stress is based on the assumption of an elastic substrate [69] (Ahmed's main work involved improving this model to make it applicable to elastoplastic substrates and plastic deformation [57]), thus a substrate with a high yield strength is more conducive to obtaining accurate results. In addition, the substrate should be a ductile material to ensure sufficient deformation that causes the hard coating to crack and form multiple cracks, and to prevent crack propagation into the substrate.

There are some other limitations. The coating needs to be a dense hard coating (porous coatings like thermal barrier coatings are not suitable) to meet the requirements of linear elastic fracture mechanics. The properties of the coating must also remain stable. This

primarily refers to materials with metastable structures that may undergo structural changes during the tensile process, leading to alterations in properties and, consequently, significant deviations in the measurement results.

6. Testing procedure of this method

Based on the discussion of the SDSS model and strategy, we have formulated a suitable procedure for measuring toughness. The measurement steps are as follows: (1) Prepare 3 or more samples, with the quantity being preferable in greater numbers. (2) Obtain the prerequisite parameters required for calculations. The necessary parameters for toughness calculation include the thickness, Poisson's ratio, Young's modulus, and yield strength (only for the substrate) of both the substrate and the coating. Residual stress can be measured or not, but it is advisable to measure it. (3) Apply different strains to each sample. The criteria for strain selection can refer to the one used in Section 5.1 for Group D, which is to have a range of crack spacings. To achieve this, increase the span of applied strain while ensuring that the minimum strain can still cause the coating to crack. If there are more samples, the span of applied strain can be appropriately reduced. (4) After unloading the samples, statistically determine the average crack spacing near the center of the coating surface. Pay attention to finding areas with dense cracks in the center and nearby areas of the coating for statistical purposes. (5) Calculate the fracture toughness. If the residual stress is unknown, try different residual stresses to minimize the deviation in toughness values between samples. Details can be referred to Section 4.3.

7. Conclusions

In conclusion, a novel model was established to determine coating toughness from changes in crack spacing under uniaxial tension. A simple, cost-effective uniaxial tensile test method was proposed, suitable for dense, hard coatings with good film-substrate bonding and thickness within 5 Î¼m. The method provides consistent results with micro-cantilever beam methods used in literature for tested coatings using TiN coatings, and its versatility was demonstrated with diamond and a-C:H coatings. The method proved stable under varying applied strain, overcoming the limitations of traditional methods. It is capable of assessing the residual stress and fracture toughness of coatings without knowledge of the residual stress, with minimal deviation. However, the model and method still have many imperfections and require further in-depth research for improvement.

CRediT authorship contribution statement

Shaoyu Wu: Writing – review & editing, Writing – original draft, Visualization, Validation, Methodology, Investigation, Formal analysis, Data curation, Conceptualization. **Shani Yang:** Writing – review & editing, Validation, Conceptualization. **Pu Geng:** Writing – review & editing, Methodology. **Kewei Gao:** Writing – review & editing, Resources. **Alex A. Volinsky:** Writing – review & editing. **Xiaolu Pang:** Writing – review & editing, Supervision, Resources, Funding acquisition, Conceptualization.

Declaration of competing interest

The authors declare that they have no known competing financial interests or personal relationships that could have appeared to influence the work reported in this paper.

Data availability

Data will be made available on request.

Acknowledgments

The authors acknowledge support from the National Natural Science Foundation of China (No. U21A2044), Science Center for Gas Turbine Project (Nos. P2021-A-IV-002-001, P2022-B-IV-008-001).

References

[1] Zhang X, Tian X, Gong C, Liu X, Li J. Effect of plasma nitriding substrate current density on the adhesion strength of *in situ* PVD TiN coatings. J Vac Sci Technol A 2023;41:033405. https://doi.org/10.1116/6.0002353.
[2] Kumar A, Mulik RS. Structure-Dependent Tribological Investigation of Hierarchically ZrN-Coated Low-Carbon Steel for Automotive Applications. J Mater Eng Perform 2024;33:2330–48. https://doi.org/10.1007/s11665-023-08123-w.
[3] Chen H, Xu G, Jin C, Wu J, Xiong L, Li X, et al. Preparation of SiOx@C via CVD method as anode materials for high-performance lithium-ion batteries. Mater Lett 2023;341:134192. https://doi.org/10.1016/j.matlet.2023.134192.
[4] Pandey K, Datta S. Performance of Si-doped TiAlxN supernitride coated carbide tool during dry machining of Inconel 718 superalloy. J Manuf Processes 2022; 84:1258–73. https://doi.org/10.1016/j.jmapro.2022.10.078.
[5] Wang A-N, Yu G-P, Huang J-H. Fracture toughness measurement on TiN hard coatings using internal energy induced cracking. Surf Coat Technol 2014;239: 20–7. https://doi.org/10.1016/j.surfcoat.2013.11.010.
[6] Hu J, Yang Q, Zhu S, Zhang Y, Yan D, Gan K, et al. Superhard bulk high-entropy carbides with enhanced toughness via metastable in-situ particles. Nat Commun 2022;14:5717. https://doi.org/10.1038/s41467-023-41481-6.
[7] Yue Y, Gao Y, Hu W, Xu B, Wang J, Zhang X, et al. Hierarchically structured diamond composite with exceptional toughness. Nature 2020;582:370–4. https://doi.org/10.1038/s41586-020-2361-2.

[8] Buchinger J, Koutná N, Kirnbauer A, Holec D, Mayrhofer PH. Heavy-element-alloying for toughness enhancement of hard nitrides on the example Ti-W-N. Acta Mater 2022;231:117897. https://doi.org/10.1016/j.actamat.2022.117897.

[9] Huang J-H, Wei L-J, Ting I-S. Evaluation of fracture toughness of VN hard coatings: Effect of preferred orientation. Mater Chem Phys 2022;275:125253. https://doi.org/10.1016/j.matchemphys.2021.125253.

[10] Csanádi T, Németh D, Lofaj F. Mechanical Properties of Hard W-C Coating on Steel Substrate Deduced from Nanoindentation and Finite Element Modeling. Exp Mech 2017;57:1057–69. https://doi.org/10.1007/s11340-016-0190-x.

[11] Kitamura T, Sumigawa T, Shimada T, Lich LV. Challenge toward nanometer scale fracture mechanics. Eng Fract Mech 2018;187:33–44. https://doi.org/10.1016/j.engfracmech.2017.10.009.

[12] Pippan R, Wurster S, Kiener D. Fracture mechanics of micro samples: Fundamental considerations. Mater Design 2018;159:252–67. https://doi.org/10.1016/j.matdes.2018.09.004.

[13] Kainz C, Schalk N, Tkadletz M, Mitterer C, Czettl C. The effect of B and C addition on microstructure and mechanical properties of TiN hard coatings grown by chemical vapor deposition. Thin Solid Films 2019;688:137283. https://doi.org/10.1016/j.tsf.2019.05.002.

[14] Zeilinger A, Daniel R, Stefenelli M, Sartory B, Chitu L, Burghammer M, et al. Mechanical property enhancement in laminates through control of morphology and crystal orientation. J Phys D: Appl Phys 2015;48:295303. https://doi.org/10.1088/0022-3727/48/29/295303.

[15] Massl S, Thomma W, Keckes J, Pippan R. Investigation of fracture properties of magnetron-sputtered TiN films by means of a FIB-based cantilever bending technique. Acta Mater 2009;57:1768–76. https://doi.org/10.1016/j.actamat.2008.12.018.

[16] Azizpour A, Hahn R, Klimashin FF, Wojcik T, Poursaeidi E, Mayrhofer PH. Deformation and Cracking Mechanism in CrN/TiN Multilayer Coatings. Coatings 2019;9:363. https://doi.org/10.3390/coatings9060363.

[17] Bartosik M, Böhm HJ, Krywka C, Zhang ZL, Mayrhofer PH. Influence of phase transformation on the damage tolerance of Ti-Al-N coatings. Vacuum 2018;155:153–7. https://doi.org/10.1016/j.vacuum.2018.06.001.

[18] Lawn BR, Evans AG, Marshall DB. Elastic/Plastic Indentation Damage in Ceramics: The Median/Radial Crack System. J Am Ceram 1980;63:574–81. https://doi.org/10.1111/j.1151-2916.1980.tb10768.x.

[19] Anstis GR, Chantikul P, Lawn BR, Marshall DB. A Critical Evaluation of Indentation Techniques for Measuring Fracture Toughness: I. Direct Crack Measurements J Am Ceram 1981;64:533–8. https://doi.org/10.1111/j.1151-2916.1981.tb10320.x.

[20] Lankford J. Threshold microfracture during elastic-plastic indentation of ceramics. J Mater Sci 1981;16:1177–82. https://doi.org/10.1007/BF01033828.

[21] Xie C, Tong W. Cracking and decohesion of a thin Al2O3 film on a ductile Al–5%Mg substrate. Acta Mater 2005;53:477–85. https://doi.org/10.1016/j.actamat.2004.10.005.

[22] Hou Y, Liu T, He D, Li Z, Chen L, Su H, et al. Sustaining strength-ductility synergy of SLM Fe50Mn30Co10Cr10 metastable high-entropy alloy by Si addition. Intermetallics 2022;145:107565. https://doi.org/10.1016/j.intermet.2022.107565.

[23] Yuan Z, Han Y, Zang S, Chen J, He G, Chai Y, et al. Damage evolution behavior of TiN/Ti multilayer coatings under high-speed impact conditions. Surf Coat Technol 2021;426:127807. https://doi.org/10.1016/j.surfcoat.2021.127807.

[24] Beuth JL. Cracking of thin bonded films in residual tension. Int J Solids Structures 1992;29:1657–75. https://doi.org/10.1016/0020-7683(92)90015-L.

[25] Chen Z, Cotterell B, Wang W. The fracture of brittle thin films on compliant substrates in flexible displays. Eng Fract Mech 2002;69:597–603. https://doi.org/10.1016/S0013-7944(01)00104-7.

[26] Harry E, Rouzaud A, Ignat M, Juliet P. Mechanical properties of W and W(C) thin films: Young's modulus, fracture toughness and adhesion. Thin Solid Films 1998;332:195–201. https://doi.org/10.1016/S0040-6090(98)01056-6.

[27] Bernoulli D, Häfliger K, Thorwarth K, Thorwarth G, Hauert R, Spolenak R. Cohesive and adhesive failure of hard and brittle films on ductile metallic substrates: A film thickness size effect analysis of the model system hydrogenated diamond-like carbon (a-C:H) on Ti substrates. Acta Mater 2015;83:29–36. https://doi.org/10.1016/j.actamat.2014.09.044.

[28] Thouless MD, Kitamura T, Sumigawa T, Shimada T, Lich LV. Crack Spacing in Brittle Films on Elastic Substrates. J Am Ceram 1990;73:2144–6. https://doi.org/10.1111/j.1151-2916.1990.tb05290.x.

[29] Thouless MD, Olsson E, Gupta A. Cracking of brittle films on elastic substrates. Acta Metall Mater 1992;40:1287–92. https://doi.org/10.1016/0956-7151(92)90429-I.

[30] Xia ZC, Hutchinson JW. Crack patterns in thin films. J Mech Phys Solids 2000;48:1107–31. https://doi.org/10.1016/S0022-5096(99)00081-2.

[31] Chen FL, He X, Prieto-Muñoz PA, Yin HM. Opening-mode fractures of a brittle coating bonded to an elasto-plastic substrate. Int J Plast 2015;67:171–91. https://doi.org/10.1016/j.ijplas.2014.10.007.

[32] Zhang C, Chen F, Gray MH, Tirawat R, Larsen RE. An elasto-plastic solution for channel cracking of brittle coating on polymer substrate. Int J Solids Structures 2017;120:125–36. https://doi.org/10.1016/j.ijsolstr.2017.04.033.

[33] Chen BF, Hwang J, Yu GP, Huang JH. In situ observation of the cracking behavior of TiN coating on 304 stainless steel subjected to tensile strain. Thin Solid Films 1999;352:173–8. https://doi.org/10.1016/S0040-6090(99)00342-9.

[34] Wiklund U, Bromark M, Larsson M, Hedenqvist P, Hogmark S. Cracking resistance of thin hard coatings estimated by four-point bending. Surf Coat Technol 1997;91:57–63. https://doi.org/10.1016/S0257-8972(96)03123-4.

[35] Ito T, Tanaka K, Akiniwa Y, Ishii T, Miki Y. X-ray study of mechanical properties of TiN thin films coated on steel by ion beam mixing method. JSME Int J, Ser A 2003;46:86–92. https://doi.org/10.1299/jsmea.46.86.

[36] Mishra AK, Gopalan H, Hans M, Kirchlechner C, Schneider JM, Dehm G, et al. Strategies for damage tolerance enhancement in metal/ceramic thin films: Lessons learned from Ti/TiN. Acta Mater 2022;228:117777. https://doi.org/10.1016/j.actamat.2022.117777.

[37] Hu Y, Huang J-H, Zuo J-M. In situ characterization of fracture toughness and dynamics of nanocrystalline titanium nitride films. J Mater Res 2016;31:370–9. https://doi.org/10.1557/jmr.2016.4.

[38] Buchinger J, Löfler L, Ast J, Wagner A, Chen Z, Michler J, et al. Fracture properties of thin film TiN at elevated temperatures. Mater Design 2020;194:108885. https://doi.org/10.1016/j.matdes.2020.108885.

[39] Zhang Z, Ghasemi A, Koutná N, Xu Z, Grünstäudl T, Song K, et al. Correlating point defects with mechanical properties in nanocrystalline TiN thin films. Mater Design 2021;207:109844. https://doi.org/10.1016/j.matdes.2021.109844.

[40] Buchinger J, Koutná N, Chen Z, Zhang Z, Mayrhofer PH, Holec D, et al. Toughness enhancement in TiN/WN superlattice thin films. Acta Mater 2019;172:18–29. https://doi.org/10.1016/j.actamat.2019.04.028.

[41] Moritz Y, Kainz C, Tkadletz M, Czettl C, Pohler M, Schalk N. Microstructure and mechanical properties of arc evaporated Ti(Al, Si)N coatings. Surf Coat Technol 2021;421:127461. https://doi.org/10.1016/j.surfcoat.2021.127461.

[42] Kainz C, Schalk N, Tkadletz M, Mitterer C, Czettl C. Microstructure and mechanical properties of CVD TiN/TiBN multilayer coatings. Surf Coat Technol 2019;370:311–9. https://doi.org/10.1016/j.surfcoat.2019.04.086.

[43] Bartosik M, Rumeau C, Hahn R, Zhang ZL, Mayrhofer PH. Fracture toughness and structural evolution in the TiAlN system upon annealing. Sci Rep 2017;7:16476. https://doi.org/10.1038/s41598-017-16751-1.

[44] Radziejewska J, Sarzyński A, Strzelec M, Diduszko R, Hoffman J. Evaluation of residual stress and adhesion of Ti and TiN PVD films by laser spallation technique. Opt Laser Technol 2018;104:140–7. https://doi.org/10.1016/j.optlastec.2018.02.014.

[45] Mei F, Sui GZ, Gong MF. Residual Stress Analysis in Different Thickness TiN Coatings on High-Speed-Steel Substrates. AMR 2014;239–242:2331–5. https://doi.org/10.4028/www.scientific.net/AMR.239-242.2331.

[46] Cao CL, Zhang XL, Dong CF, Zha X. Effect of Annealing on Properties of the TiN & TiAlN Coatings Deposited on Powder Metallurgy High Speed Steel (S790). Appl Mech Mater 2014;477–478:1397–402. https://doi.org/10.4028/www.scientific.net/AMM.477-478.1397.

[47] Dericioglu AF. Effect of Microstructure on the Mechanical Behavior of Reactive Magnetron Sputtered Al2O3/TiO2 Multilayer Ceramics. Mater Trans 2008;49:2714–22. https://doi.org/10.2320/matertrans.MER2008055.

[48] Berger M. Thick Physical Vapour Deposited TiB_2 Coatings. Surf Eng 2002;18:219–23. https://doi.org/10.1179/026708402225005304.

[49] Du S, Zhang K, Wen M, Ren P, Meng Q, Hu C, et al. Tribochemistry dependent tribological behavior of superhard TaC/SiC multilayer films. Surf Coat Technol 2018;337:492–500. https://doi.org/10.1016/j.surfcoat.2018.01.064.
[50] Morasch KR, Bahr DF. An energy method to analyze through thickness thin film fracture during indentation. Thin Solid Films 2007;515:3298–304. https://doi.org/10.1016/j.tsf.2006.01.043.
[51] Chen J, He G, Han Y, Yuan Z, Li Z, Zhang Z, et al. Structural toughness and interfacial effects of multilayer TiN erosion-resistant coatings based on high strain rate repeated impact loads. Ceram Int 2021;47:27660–7. https://doi.org/10.1016/j.ceramint.2021.06.190.
[52] Bull SJ. Microstructure and indentation response of TiN coatings: The effect of measurement method. Thin Solid Films 2019;688:137452. https://doi.org/10.1016/j.tsf.2019.137452.
[53] Lawn BR. Fracture of brittle solids. 2nd ed. Cambridge; New York: Cambridge University Press; 1993.
[54] Agrawal DC, Raj R. Measurement of the ultimate shear strength of a metal-ceramic interface. Acta Metall 1989;37:1265–70. https://doi.org/10.1016/0001-6160(89)90120-X.
[55] Huang J, Kim BC, Takayama S, Thouless MD. The control of crack arrays in thin films. J Mater Sci 2014;49:255–68. https://doi.org/10.1007/s10853-013-7700-3.
[56] Jansson NE, Leterrier Y, Medico L, Månson JAE. Calculation of adhesive and cohesive fracture toughness of a thin brittle coating on a polymer substrate. Thin Solid Films 2006;515:2097–105. https://doi.org/10.1016/j.tsf.2006.07.012.
[57] Ahmed F, Bayerlein K, Rosiwal SM, Göken M, Durst K. Stress evolution and cracking of crystalline diamond thin films on ductile titanium substrate: Analysis by micro-Raman spectroscopy and analytical modelling. Acta Mater 2011;59:5422–33. https://doi.org/10.1016/j.actamat.2011.05.015.
[58] Thouless MD, Li Z, Douville NJ, Takayama S. Periodic cracking of films supported on compliant substrates. J Mech Phys Solids 2011;59:1927–37. https://doi.org/10.1016/j.jmps.2011.04.009.
[59] Oliver WC, Pharr GM. An improved technique for determining hardness and elastic modulus using load and displacement sensing indentation experiments. J Mater Res 1992;7:1564–83. https://doi.org/10.1557/JMR.1992.1564.
[60] Rehman H, ur, Ahmed F, Schmid C, Schaufler J, Durst K.. Study on the deformation mechanics of hard brittle coatings on ductile substrates using in-situ tensile testing and cohesive zone FEM modeling. Surf Coat Technol 2012;207:163–9. https://doi.org/10.1016/j.surfcoat.2012.06.049.
[61] Tavares da Costa MV, Bolinsson J, Neagu RC, Fayet P, Gamstedt EK. Experimental assessment of micromechanical models for fragmentation analysis of thin metal oxide coatings on polymer films under uniaxial tensile deformation. Surf Coat Technol 2019;370:374–83. https://doi.org/10.1016/j.surfcoat.2019.03.035.
[62] Schaufler J, Durst K, Massler O, Göken M. In-situ investigation on the deformation and damage behaviour of diamond-like carbon coated thin films under uniaxial loading. Thin Solid Films 2009;517:1681–5. https://doi.org/10.1016/j.tsf.2008.09.104.
[63] Davies AR, Field JE, Takahashi K, Hada K. The toughness of free-standing CVD diamond. J Mater Sci 2004;39:1571–4. https://doi.org/10.1023/B:JMSC.0000016153.90600.a6.
[64] Lu FX, Jiang Z, Tang WZ, Huang TB, Liu JM. Accurate measurement of strength and fracture toughness for miniature-size thick diamond-film samples by three-point bending at constant loading rate. Diamond Relat Mater 2001;10:770–4. https://doi.org/10.1016/S0925-9635(00)00523-9.
[65] Schaufler J, Schmid C, Durst K, Göken M. Determination of the interfacial strength and fracture toughness of a-C: H coatings by in-situ microcantilever bending. Thin Solid Films 2012;522:480–4. https://doi.org/10.1016/j.tsf.2012.08.031.
[66] Guo T, Qiao L, Pang X, Volinsky AA. Brittle film-induced cracking of ductile substrates. Acta Mater 2015;99:273–80. https://doi.org/10.1016/j.actamat.2015.07.059.
[67] Handge UA. Analysis of a shear-lag model with nonlinear elastic stress transfer for sequential cracking of polymer coatings. J Mater Sci 2002;37:4775–82. https://doi.org/10.1023/A:1020814314019.
[68] Cox HL. The elasticity and strength of paper and other fibrous materials. Br J Appl Phys 1952;3:72–9. https://doi.org/10.1088/0508-3443/3/3/302.
[69] Hsueh CH, Yanaka M. Multiple film cracking in film/substrate systems with residual stresses and unidirectional loading. J Mater Sci 2003;38:1809–17. https://doi.org/10.1023/A:1023200415364.